The assessment of a mobile geo-electrical measurement system

a study on the validity and contributing factors to quantify leakage in sewer systems

Stegeman, Bram; Hoffmann, Rob; Hopman, Victor; Langeveld, Jeroen; Clemens-Meyer, François

Important note
To cite this publication, please use the final published version (if applicable).
Please check the document version above.

The assessment of a mobile geo-electrical measurement system: a study on the validity and contributing factors to quantify leakage in sewer systems

Bram Stegeman, Rob Hoffmann, Victor Hopman, Jeroen Langeveld & François Clemens-Meyer

Published online: 23 Feb 2022.

Submit your article to this journal ✎

Article views: 131

View related articles ✎

View Crossmark data ✎

Taylor & Francis
Taylor & Francis Group

RESEARCH ARTICLE

OPEN ACCESS · Check for updates

The assessment of a mobile geo-electrical measurement system: a study on the validity and contributing factors to quantify leakage in sewer systems

Bram Stegeman [ID][a], Rob Hoffmann[b], Victor Hopman[c], Jeroen Langeveld [ID][a,d] and François Clemens-Meyer [ID][b,e]

[a]Faculty of Civil Engineering and Geosciences, Department of Water Management, Delft University of Technology, Delft, The Netherlands; [b]Department of Hydraulic Engineering, Deltares, Delft, The Netherlands; [c]Department of Subsurface & Groundwater Systems, Deltares, Delft, The Netherlands; [d]Partners4urbanwater, Nijmegen, The Netherlands; [e]Faculty of Engineering, Department of Civil and Environmental Engineering, Norwegian University of Science and Technology, Trondheim, Norway

ABSTRACT
The main application of the mobile geo-electrical measurement is the detection of the presence and determining the location of leakage in sewer systems. To do so, this method relies on the increase in the measured electrical current between an electrode inside and an electrode outside the sewer system. To use this technique for the quantification of leakages further assumptions on the measured current are required. In this study, a model to simulate the geo-electrical measurement system is developed. Laboratory experiments are conducted to investigate the influence and contribution of the model components on the measured current and the validity of the assumptions. The experimental results demonstrate that multiple components significantly contribute to the measured current apart from the leakage in the pipe. As a consequence, the properties of the leakage in the pipe are likely to be significantly under- or overestimated in most measuring systems currently applied in practice.

Introduction

The in- and exfiltration of (waste) water in urban drainage systems is one of the main defects occurring in these ageing systems (Tscheikner-Gratl et al. 2019). On one hand, exfiltration poses a potential risk on the contamination of groundwater. On the other hand, infiltration may induce a significantly increased hydraulic load on wastewater treatment plants (WWTP's) inducing capacity and efficiency reduction and, next to that, the occurrence of sinkholes is also a known consequence of infiltration (e.g. Davies et al. 2001; Stanić, Langeveld, and Clemens 2014; Lee et al. 2015).

On the scale of an urban catchment, a range of methods has been developed and applied to quantify the amount of infiltration (e.g. Weiß, Brombach, and Haller 2002; De Bénédittis and Bertrand-Krajewski 2005a; De Bénédittis and Bertrand-Krajewski 2005b; Zhang et al. 2018; Zhao et al. 2020). The need for relatively few and simple data is an advantage of these methods. However, when information is needed on a smaller scale, difficulties arise to obtain reliable estimates for the location of a leak and the in- or exfiltrating quantities. The application of tracer-based methods to quantify exfiltration in a stretch of conduits has been reported in the literature (Rieckermann et al. 2007). Identifying the exact location of the in- or exfiltration is more cumbersome to achieve. Fibre optic DTS cables can be used to localize infiltration (Hoes et al. 2009; Beheshti and Sægrov 2018; Panasiuk et al. 2019), and can potentially also detect and locate exfiltration. This method, however, requires the installation of a fibre optic cable in- and/or outside the pipe. Visual inspection (CCTV) of urban drainage systems is less labour intensive than the latter, but is known to suffer from biased, inaccurate and incomplete information

(Dirksen et al. 2013). Apart from that it is very likely that, especially exfiltration, is easily 'missed' using this method of assessment as it can only indirectly be observed (e.g. when a crack is observed it is assumed this may give way to exfiltration, however, the latter cannot be observed directly).

Geo-electrical measurements can be used to detect and locate in- and exfiltration. A mobile geo-electrical measurement method that measures the electrical current between an electrode in the pipe and an electrode (i.e. grounding pin) in the surrounding soil (e.g. ASTM 2018) has already been applied in practice for some decades. In the measuring set-up an electric potential is applied between a mobile electrode in the pipeline and a stationary electrode at the surface. While the electrode is moved through the (partially) water-filled pipeline, the electrical current and the position are recorded. Subsequently, any changes in the measured current are related to changes in impedances in the electrical circuit. The leakage in the pipeline (induced by e.g. a crack, a hole or a defect joint) and the resulting in- or exfiltration creates a local decrease in impedance; hence, an increase in current is obtained. This is illustrated in the current-position diagram in Figure 1.

For the mobile geo-electrical measurement system, a range of electrode configurations are described in literature. In its simplest form, it is one electrode in the pipeline and one electrode on ground level; also referred to as the 'mise-a-la-masse' method (Wood and Palmer 2000). More advanced configurations consist of three conductive electrodes grouped in a cylinder with a mutual axis, commonly referred to as 'the probe'. While the central electrode is referred to as the measurement electrode; the outer electrodes are called the shield

---
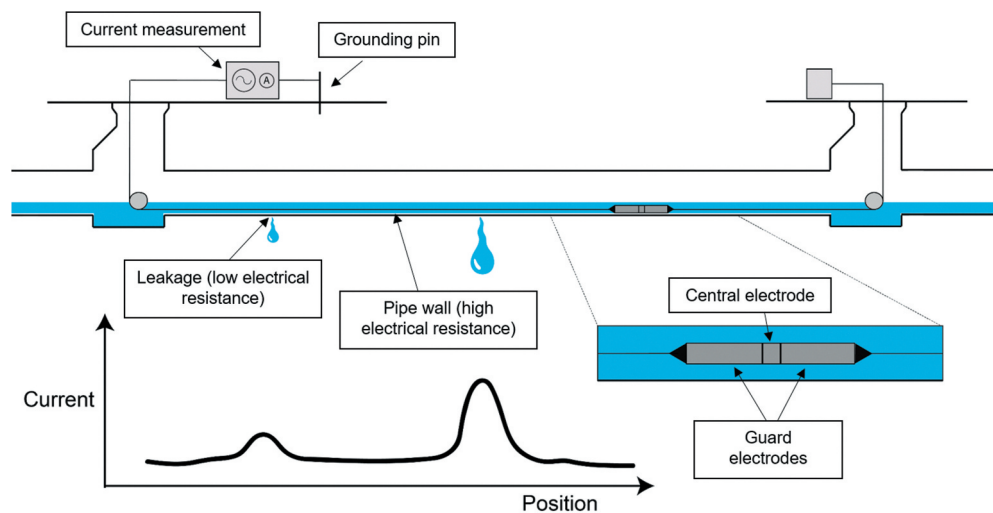
Figure 1. The measurement principle of a mobile geo-electrical measurement system. The current-position diagram indicates the position of possible leakages.

or guard electrodes, see Figure 1. These electrodes have the purpose to screen the central electrode from the environment in the pipe. In this way the electrical field of the central electrode is to a certain extent isolated from the outer impedances of the pipe increasing the sensitivity of the set-up to lateral changes in impedances. This configuration is known as the Focused Electrode Leak Localization set-up or FELL (e.g. Gokhale and Graham 2004; ASTM 2018; Wolf 2003). This configuration is also used in geophysical applications like borehole logging (Selley and Sonnenberg 2015).

The main application of the mobile geo-electrical measurement in buried pipelines is the detection of the presence and determining the location of in- and exfiltration in underground (waste) water systems (e.g. Selvakumar et al. 2014; Malik 2019; Henley and Hansen 2019). Quantification of the potential leak discharge is mentioned by (Moy, Wilmut, and Harris 2012), who claim that the focussed geo-electrical measurement can also be used to estimate the potential leak discharge in pipes below the groundwater table. To quantify the potential leak discharge, assumptions are made with respect to water depth above the top of the pipe (fixed at 308 mm) and that the defect is a crack with a fixed width (0.635 mm). It is stated that under these conditions the measurements have shown that water will flow into the pipe at the rate of 0.0012 l/s/mm^2. Subsequently, the potential leak discharge is calculated with the cross-sectional area of the defect, which is derived from the focussed geo-electrical measurement. Hence, the quantification depends on the validity of two major underlying implicit assumptions:

- The change in the current due to a leakage in the pipe can be attributed to the electrical resistance of the leakage;
- The electrical resistance of the leakage is related to the dimensions of the leakage.

Assuming homogenous conditions in electrical conductivity, pipe wall thickness and cross-sectional area, the second assumption is applicable to quantify the defect area. This, however, requires the electrical resistance of the leakage to be known from the first assumption.

To the authors' knowledge an independent experimental validation of the first assumption has not been reported in literature to date, therefore an experimental set-up is build and presented in Section 2 of this article. In this section, a model to simulate the geo-electrical measurement system is presented as well. The experimental results; the electrical current, resistance and capacitance of the individual model components are presented in Section 3 along with the electrical resistance of the leakage as measured using 21 experimental measurement geometries. Section 4 discusses the results and finally, the main conclusions are presented in Section 5.

Model, materials and methods

Model

A model to simulate the geo-electrical measurement system has been developed, as shown in Figure 2. The model is implemented in a Matlab ® (2019b) script and is used to simulate the electrical current flowing through the network. The model equations are presented in Appendix A. The required model input are admittances and the applied electrical potential between the electrodes. The voltage follower is implemented in the model as well.

The electrical current measured is the result of the combined effect of the individual components in the electrical circuit. These components in the circuit are defined as:

- Ymm is the shunt resistor. In parallel to the shunt resistor is the cable-capacitance. The latter is formed between the central cable conductor and the two cable conductors feeding the outer electrodes. In addition, the capacitance is also formed between the central cable conductor and the cable shielding/the environment;
- Ylm and Yrm are formed by the electrical conductivity in the water between the central and the outer electrodes as well as the capacitances between the three electrodes and capacitances between the cable-conductors;
- Ymh, Ylh, Yrh are, respectively, the electrical conductivity in the water between the central, left or right electrode and the upper area of the leakage.
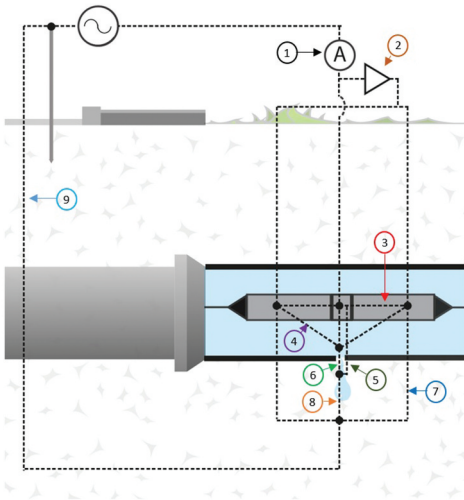
Figure 2. The model; an electrical circuit of the geo-electrical measurement system. The left side shows the nodes and their mutual connections, the right side shows how the admittances are related in a typical field application. The corresponding colours and numbers indicate the links between the components on both sides of the figure.

- Yh is the admittance of the leakage. This is the electrical conductivity of the soil/water in the leakage;
- Yms is the electrical conductivity and capacitance between the central electrode and the soil around the leakage in the vicinity of the pipe;
- Y_s is the admittance of the soil between the leakage and the deeper soil layers around the pipe. This is the electrical conductivity of the soil between the leakage and the soil further away from the leakage;
- Yld and Yrd are respectively the electrical conductivity and the capacitance between the outer left or the outer right electrode and the soil further away from the area around the leakage in the pipe;
- Yds is the electrical conductivity in the soil layers further away from the leakage in series with the grounding pin connected to the return of the generator;
- Yia is the input admittance of the voltage follower.

The admittance of the leakage (Yh) is of main interest because it holds potential information on the leakage dimensions. To uniquely identify the admittance of the leakage, the characteristics of all other components should either be known to a certain degree of accuracy and precision or they should a priori be known to have a negligible influence on the measuring result. In practice however, several of these components are unknown. Hence, strictly mathematical speaking, the model equations cannot be solved for the unknown admittance of the leakage. Consequently, relaxation of the demand on the required information will result in a systematic error in the estimate of the admittance of the leakage and the derived properties such as the leakage area. To which extent this is so, also depends on the contribution of the different components to the measured current. To quantify this, research as described in the following sections is performed.

Materials

Experimental set-up

The experimental set-up comprises 4 main components: a polyethylene (PE) tank containing sand, a PVC sewer pipe filled with water, a moving platform to vary the position of the probe in the pipe and a geo-electrical measurement system.

Sand filled tank. The PE tank is filled with a layer of gravel and a layer of sand separated by geotextile. The gravel embeds a drainage construction, referred to as the bottom layer while the top layer consists of sand typically used as filling material at sewer constructions. The water level of the main tank is controlled, allowing to mimic different groundwater levels. The ground temperature, water level, water temperature and water conductivity are monitored separately. A schematic overview and the layout of the experimental set-up are presented in Figures 3 and 4.

PVC sewer pipe. A PVC pipe (external Ø 20 cm, wall thickness 0.5 cm, length 196 cm) is installed horizontally in the main tank. The crown of the pipe is removed to allow access for measurements. At the bottom of the pipe a leakage is created with the geometry of a circular hole (Ø 1 cm). The water depth in the pipe is kept constant; water is added continuously with a controlled pump to compensate for the leakage. Abundant water will return to the water tank via an overflow construction. The water depth in the sewer pipe, water temperature and conductivity are measured at the start of and after finalizing an experimental run.

Moving platform. A moving platform is placed on top of the tank to move the probe aligned through the pipe. The probe is placed in a suspension construction to alter the vertical

1 Moving platform
2 Suspension construction
3 Main tank
4 Transparent PVC pipe
5 Water tank with pump
6 Flow control

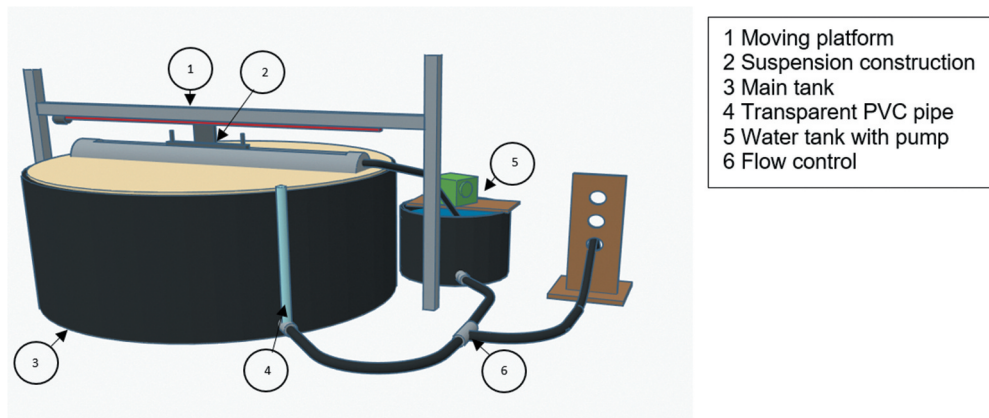**Figure 3.** A 3D schematic overview of the experimental set-up.

Figure 4. An overview of the experimental set-up.

1 Central measurement unit
2 Electrode inside the pipe (Ø 1 cm)
3 Electrode outside the pipe (Ø 1 cm)
4 Electrode in the sand layer (1 x 1 cm)
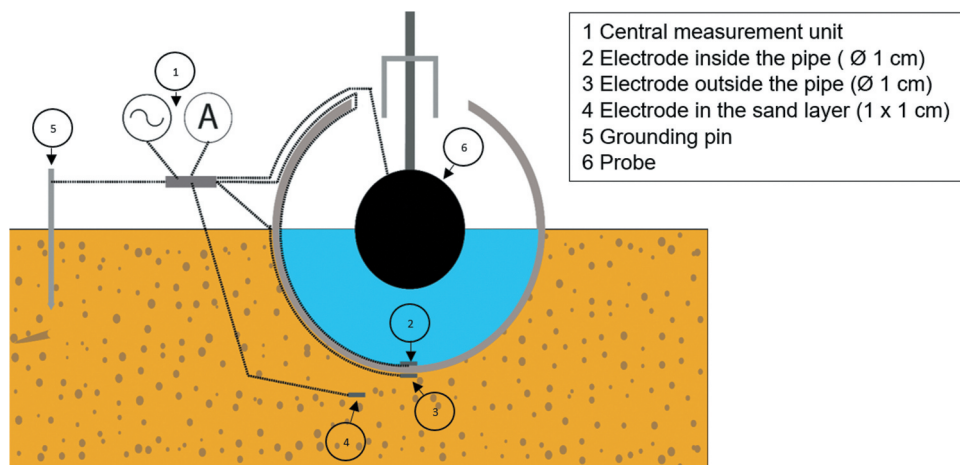5 Grounding pin
6 Probe

Figure 5. The electrodes in the measuring set-up.

Table 1. The electrode pairs used in the experimental set-up to determine admittances.

Electrode pair[a]	Parameters obtained	Input model component
2 + 6	Current, resistance and capacitance between the probe and the leakage	Ymh, Ylh, Yrh
3 + 5	Current, resistance and capacitance of the soil between the leakage and the grounding pin	Yds
5 + 6	Current, resistance and capacitance between the probe and the grounding pin	Total
4 + 5	Current between the electrode in the sand layer and the grounding pin (soil bulk current)	-

[a]see Figure 5.

position of the probe, see Figure 3. The speed (max 7.5 cm/s) and the horizontal position of the probe is controlled and recorded.

Geo-electrical measurement system.
The geo-electrical measurement system contains two main parts: (1) a central unit to measure the current between (2) a pair of stainless-steel electrodes. The central unit consists of a function generator and a shunt resistor to measure the electrical current between two electrodes. To this end the obtained voltage across the resistor is amplified and recorded. Different electrode pairs can be mounted to the central unit to determine different admittances (see Figure 5 and Table 1). Only one pair of electrodes can be mounted to the system at a time. Consequently, the resistance and capacitance of each individual admittance is measured separately and not simultaneously. This also applies to the components Ymh (the admittance between the central electrode and the leakage), Ylh and Yrh (the admittance between the outer electrodes and the leakage). Depending on the component, the current flow at one of the electrodes of probe is measured and the voltage follower is connected to the other electrodes of the probe.

The design of the probe electrodes is based on literature (e.g. Martel, Feeney, and Tuccillo 2011). The used probe consists of three cylindrical shaped electrodes (diameter 7 cm) aligned in a mutual axis being isolated by plastic compartments (maximum diameter 7.5 cm). The outer electrodes have a length of 24.7 cm, while the central has a length of 6.5 cm.

Data acquisition
The equipment is directly connected to a data acquisition system: a computer-controlled A-D Converter to ensure synchronisation.

Laboratory experiments

The laboratory experiments have been done at 21 measurement geometries. These geometries are selected based on preliminary experiments in which controllable parameters were changed to assess the sensitivity of the results. Subsequently, the parameters for which the results were relatively sensitive have been varied in the measurement geometries. While the controlled speed of the probe was fixed at 5.0 cm/s for each experiment, the vertical distance of the bottom of the probe with respect to the leakage location has been tested at 7 different heights (0.015 m – 0.075 m). The

water depth in the sewer pipe remained constant at 0.11 m and the water level in the main tank varied between 32 and 33 cm below surface level to simulate exfiltration conditions. Given the stable pressure difference and the fixed dimensions of the leakage, the leak discharge is assumed to be constant and was approximately 1.9 l/min. The horizontal distance of the grounding pin with respect to the leakage location has been tested at 7 distances (0.2 m – 0.8 m) perpendicular to the pipe. The latter experiments were performed with the grounding pin at two different depths (0.3 and 0.5 m), respectively above and also partly below the groundwater level. An overview of the measurement geometries applied is presented in Appendix B.

In each measurement geometry, the admittances between the electrodes of the probe and the leakage (Ymh, Ylh and Yrh) are measured separately. The admittances between the electrodes of the probe and the surrounding soil (Yls, Yms and Yrs) are a combination of the admittance of the water, the pipe wall and the surrounding soil. While the impedance of the water and the soil will likely be in the order of 0.1–1 kΩ, the impedance of the PVC-pipe wall will likely be > 10^{10} Ω. These impedances are in parallel with the impedance of the leakage in the pipe wall which is expected to be in the order of 1–2 kΩ. Consequently, when the probe is at the leakage location, the contribution of the admittances including the pipe wall are expected to be negligible and therefore these are not taken into consideration in the experiments. The admittances between the central and the outer electrodes (Yrm and Ylm) are not considered in the experiments either: the potential of the electrodes remains the same by the voltage follower implying there is no current between the electrodes. The admittances between the leakage and the grounding pin (Ys and Yds) are jointly measured in each measurement geometry and named Yds. The model is adapted to the given situation.

Methods
Electrical current
The measurements are performed with an alternating current (AC) to prevent a charge build-up at the electrode/medium interface (i.e. polarisation).

The selection of the frequency of the alternating current depends on the conductivity and capacitance of the medium between the electrodes and other (unknown) parasitic capacitances. In this study the measurements are performed at an AC frequency of 400 Hz. This proved to be workable trade-off to decrease the contribution of the contact serial capacitance to a level of insignificance on one hand, and minimising unwanted parasitic effects on the other hand.

Data processing
The data processing consists out of four main steps. These steps are implemented in Matlab ® (2019b) scripts.

Step 1 – Amplitude and phase shift.
In the first step, the recorded time series are divided into subsections; a time window k with each holding N data points.

In each time window k, frequency, amplitude and phase of the applied potential difference over the function generator are determined with a standard build in Matlab® (2019b) function (nlinfit; a nonlinear least-squares solver). In parallel, the amplitude and the phase shift of the measured potential difference across the shunt resistor are determined using a discrete Fourier analysis (e.g. Spiegel 1974).

Step 2 – Current, resistance and capacitance.

In the second step, the current and subsequently the resistance and capacitance are determined. To do so, the electrical circuit as shown in Figure 6 is considered. The potential difference over the signal generator (V_g) and the potential difference (V_m) across the shunt resistor (R_M) are measured. Due to the selected resistance of the shunt resistor, the influence of the parallel capacitance C_M is reduced into an order so that it can be neglected. The occurring phase difference is represented by ϕ_Z. Z_M is the known impedance of the shunt resistor. R_{X1} and C_{X1} are the unknown resistance and the capacitance of the impedance (Z_X) between the two electrodes.

Using the impedance of this electrical circuit, the unknown capacitance of the medium C_{X1} is given by Equation (1). The unknown resistance (R_{X1}) is in parallel with the resistance of the voltage follower (R_{IA}). The unknown resistance of the medium (R_{X1}) is given by Equation (2) and the total resistance (R_x) is given by Equation (3) for stationary conditions.

$$C_{x1} = \frac{\sqrt{V_m^2 R_m^2 + 2V_m^2 R_m R_x + V_m^2 R_x^2 - V_g^2 R_m^2}}{R_m R_x \omega \sqrt{V_g^2 - V_m^2}} \tag{1}$$

$$R_{x1} = \frac{R_x \cdot R_{IA}}{R_{IA} - R_x} \tag{2}$$

$$R_x = -\left(\frac{R_m \cdot V_m^3 - R_m \cdot V_g^2 \cdot V_m + \kappa_3 + \tan^2(\phi_Z) \cdot R_m \cdot V_m^3 - \kappa_2 + \tan^2(\phi_Z) \cdot R_m \cdot V_g^2 \cdot V_m}{\kappa_1} \right) \tag{3}$$

Where:

$$\kappa_1 = \tan^2(\phi_Z) \cdot V_m^3 - V_g^2 \cdot V_m + V_m^3$$

$$\kappa_2 = R_m \cdot V_g \cdot V_m^2 \cdot \sqrt{\tan^2(\phi_Z) + 1}$$

$$\kappa_3 = R_m \cdot V_g^3 \cdot \sqrt{\tan^2(\phi_Z) + 1}$$

Step 3 – Uncertainty propagation.

In the third step the 95% confidence interval for the output parameters is calculated using the Monte Carlo method. In sampling, the probability distributions and the known mutual correlations between the parameters are accounted for. In the Monte Carlo process stable results of the mean, standard deviation and skewness of the parameter output distribution are obtained between 30.000 and 50.000. Therefore, a sample of 100.000 is used throughout this study.

Step 4 – Data and image export.

In the final step, for each time window k, the output data is stored and plotted against the average distance ($\overline{d_k}$) or average time ($\overline{t_k}$).

Electrical resistance of leakage

With conductive media such as (waste) water and a sand/water mixture, the capacitance is negligible and the resistance determines the electrical current. Hence, if the admittance of the leakage is known, the electrical resistance of the leakage can be determined.

Given the measurements of the individual resistances and the measured current between the central electrode and the grounding pin, the model equations are solved to quantify the electrical resistance of the leakage (Rhc). The model is calibrated at a fixed position in the sewer pipe; the central electrode of the probe is directly above (1) the leakage or (2) above the adjacent electrode inside the sewer pipe. In doing so, each individual component is represented by only one data point in the model input.

In parallel, a reference electrical resistance of the leakage (Rhr) is determined given the dimensions and resistivity of the water filling the leakage. For the latter, the dimensions of the leakage, the specific conductivity and the temperature measured in the PVC sewer pipe are used.

The 95% confidence intervals for Rhc and Rhr are quantified in line with the procedure described at step 3 of the data processing.
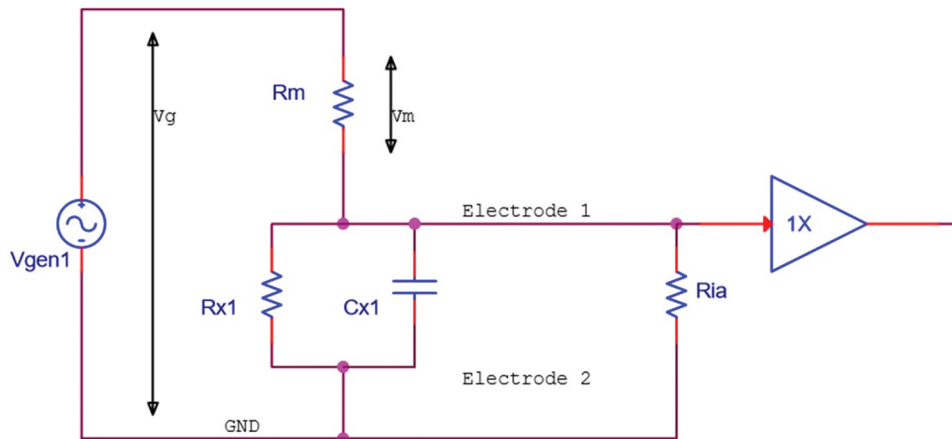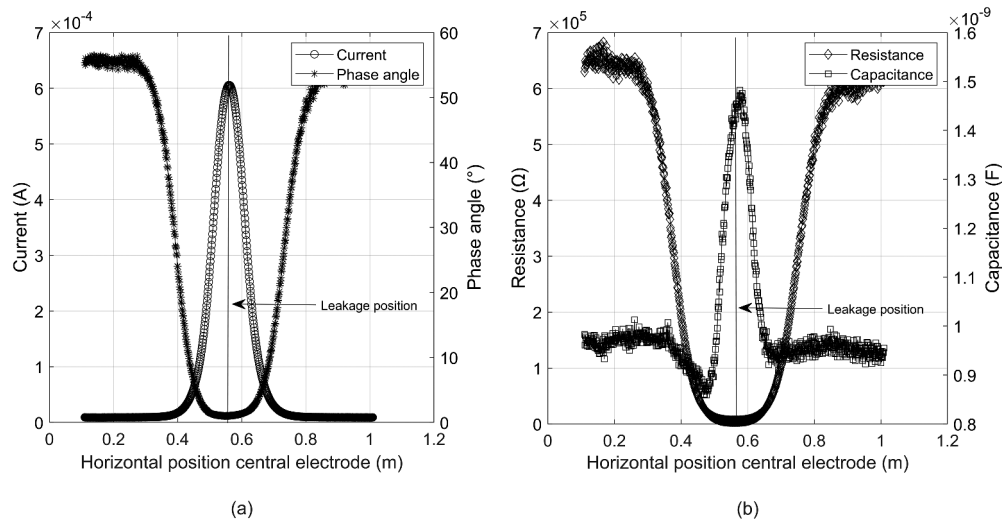

Figure 6. The electrical circuit with impedances in the experimental set-up.

Figure 7. The current and phase angle measured at Total (a). The resistance and capacitance measured at Total (b). The probe moves in a horizontal direction and is fixed at a vertical position of 0.045 m above the leakage.

## Results

Model components

Figure 7(a) presents the measured current and the phase angle between the central electrode of the probe and the grounding pin (*Total*). While the current increases towards the location of the leak, the phase angle decreases to a minimum at the location of the leak. In Figure 7(b) the resistance and the capacitance are shown. Although the capacitance increases towards the leakage location, the capacitive current is less dominant and becomes negligible at the leakage location. The results of the individual in-pipe components, the impedances between the electrodes of the probe and the leakage in the pipe wall (*Ymh, Ylh, Yrh*) show that a similar reasoning is applicable.

In Figure 8(a,b) the measured currents for *Ymh* and *Ylh* are presented at different vertical distances between the probe bottom and the leakage. At a vertical distance of 0.055 m and 0.075 m the probe is only partly submerged. A 'diffusion' like

change in the current-position diagram is observed. Consequently, the properties of the peak: the prominence and the width change.

In Figure 9 the total resistance (*Total*) and the resistance of the different components at the location of the leakage are presented at measurement geometry 1 to 7. The vertical position of the probe is projected on the x-axis. With increasing vertical distance, an increase in resistance can be observed between the central electrode and the leakage (*Ymh*) and in the total resistance between the central electrode and the grounding pin (*Total*) while the resistance between the outer electrodes and the leakage (*Ylh* and *Yrh*) decreases. The resistance between the leakage and the grounding pin (*Yds*) remains constant.

Figure 10 presents the total resistance and the resistance of the different components at the location of the leakage at different distances of the grounding pin to the leakage (measurement geometry 8 to 14). The grounding pin is above the groundwater level. With increasing distance, an increase in
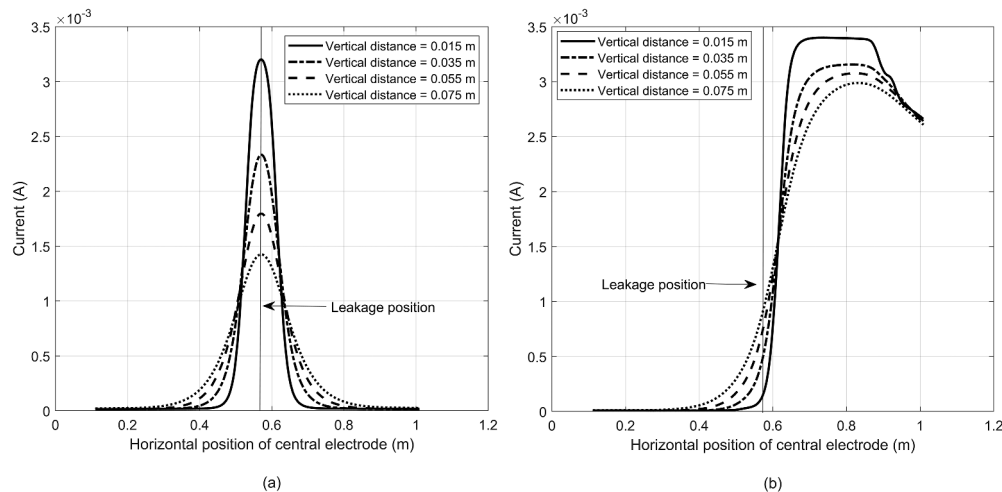
Figure 8. The current at Ymh (a) and Ylh (b) measured at different vertical distances of the probe with respect to the leakage at the bottom.
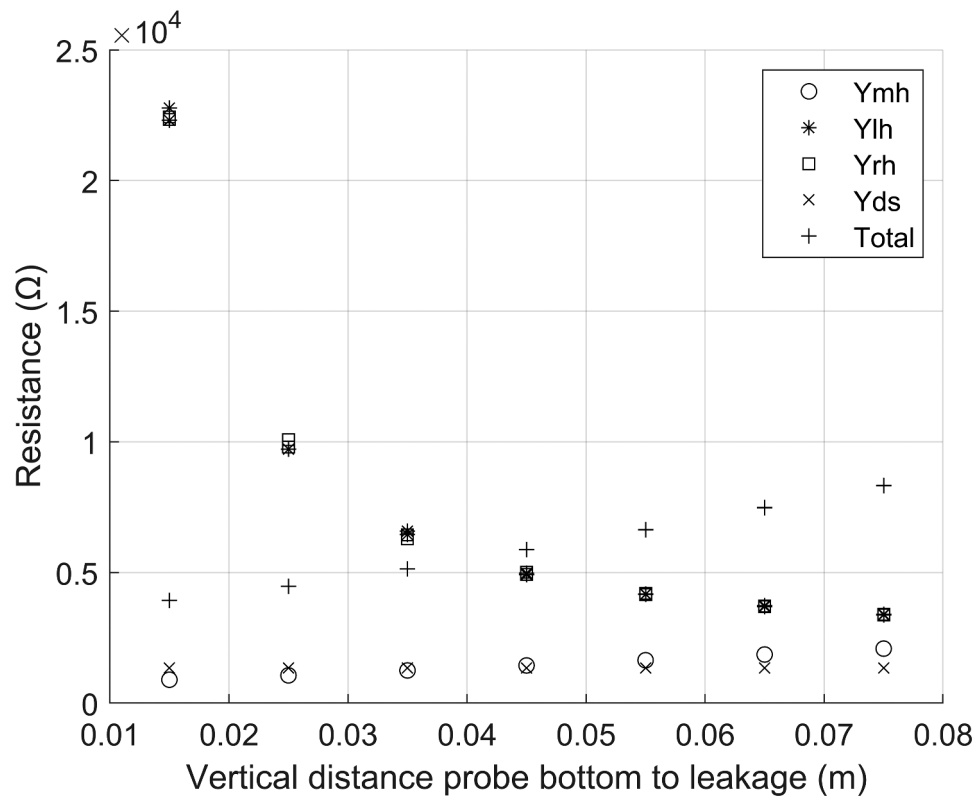
Figure 9. The total resistance and the resistance of the different components at the location of the leakage at different vertical positions of the probe.
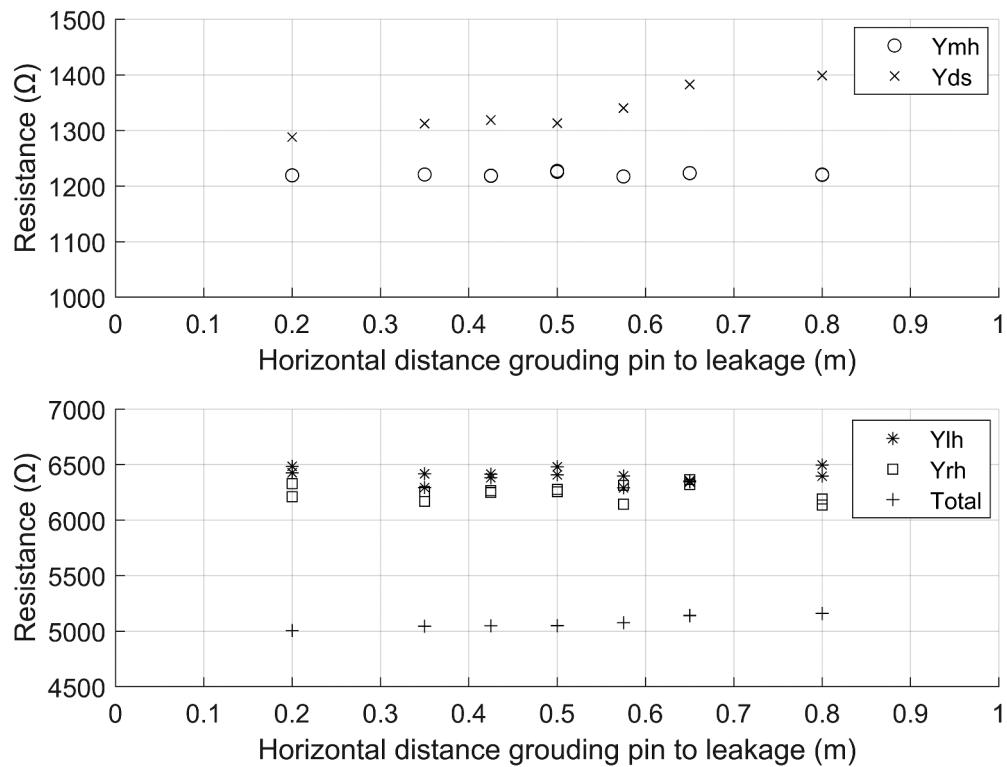

Figure 10. The total resistance and the resistance of different components at the location of the leakage at different horizontal distances between the grounding pin (above groundwater level) and the leakage.
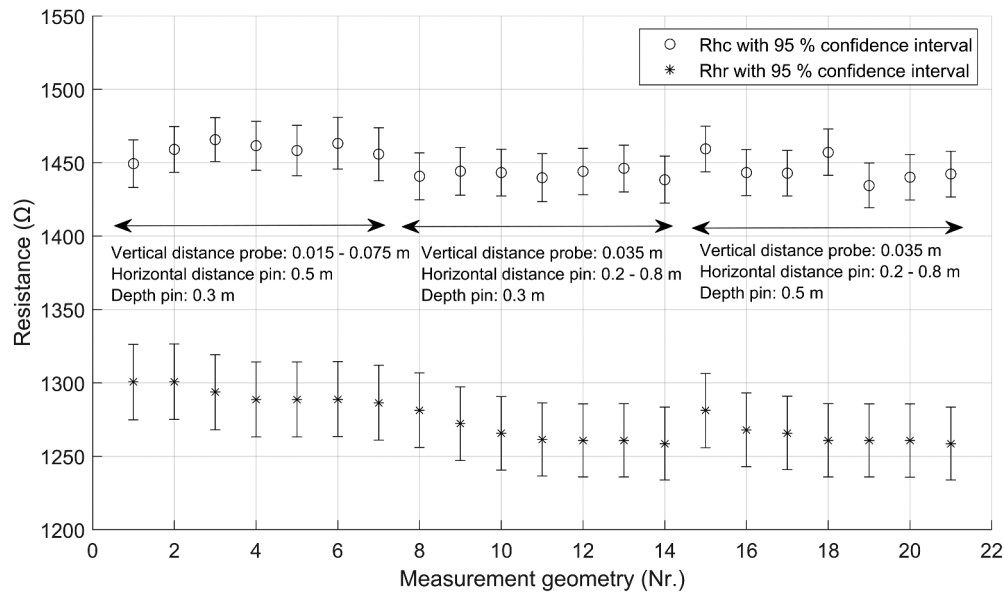
Figure 11. The calibrated electrical resistance of the leakage (Rhc) and the reference electrical resistance of the leakage (Rhr) at the measurement geometries.

resistance can be observed between the leakage and the grounding pin (*Yds*) and in the resistance between the central electrode of the probe and the grounding pin (*Total*). This while the resistances between the three electrodes of the probe and the leakage (*Ymh, Ylh* and *Yrh*) remain almost constant.

The results of the components at an intrusion depth of the grounding pin of 30 cm are largely similar to the results of the components at an intrusion depth of 50 cm (measurement geometry 15 to 21). The main differences are the reduction of resistance *Yds* (70–100 Ω) and the reduction of *Total* (110–150 Ω).

Resistance of the leakage

In Figure 11 the results of the calibrated electrical resistance of the leakage (*Rhc*) and the reference electrical resistance of the leakage (*Rhr*) are presented at the 21 measurement geometries. The difference between the two estimates of the electrical resistances of the leakages (*Rhc* and *Rhr*) ranges between 148 and 196 Ω (Pearson's ρ= 0.71).

Discussion

Electrical current

Logically, the measured current is at its highest at the leakage location. This observation is line with literature (e.g. Wolf 2003).

The shape of the current-position diagram is of main interest for the relationship between the increase in current and leakage quantification. With respect to the validity of the leakage quantification assumptions, it is required that the measured current at the leakage location only depends on the dimensions of the leakage. This has not been observed in the results of the experiments. Although not explicitly investigated, a clear dependency between the leak discharge and the measured current has also not been observed. It is

demonstrated that the shape of the current-position diagram, and the current at the leakage location, also depends on the vertical distance between the probe bottom and the leakage in the pipe wall. Thus, while the dimensions and discharge of the leakage remain constant, this study demonstrates that a smaller vertical distance to the leak results in an increased current between the central electrode and the grounding pin and a sharper peak in the current-position diagram. As expected, this is the result of the difference in the vertical distance of the probe and the interplay of the central and the outer electrodes near the leakage. If the central electrode is at the location of the leakage and the vertical distance is reduced, the resistances and their ratio will change. Therefore, the ratio of the electrical current between the different electrodes of the probe and the leakage will also change, this is also illustrated Figure 12.

If the central electrode is further away from the leakage and the vertical distance decreases, the current between the central electrode and the leakage reduces. As a result, the width of the peak in the current-position diagram decreases when the vertical distance between the probe and the leakage reduces. According to ASTM (2018) the apparatus manufacturer should be consulted regarding the relationship between the measured current and the pipe leak size and its classification. To the authors' knowledge this information is not publicly available and/or known to have been validated. Regrettably the main findings of this research could not be validated with data from other parties.

Resistance and capacitance

The resistance reaches a minimum at the leakage location while the capacitance is close to its maximum at the same location. A deviation (~2 cm) in the position of the maximum capacitance is observed, this is likely caused by inhomogeneities. This has not been investigated any further since the contribution of the capacitance is deemed to be negligible. Local inhomogeneities, due to for example void formation,
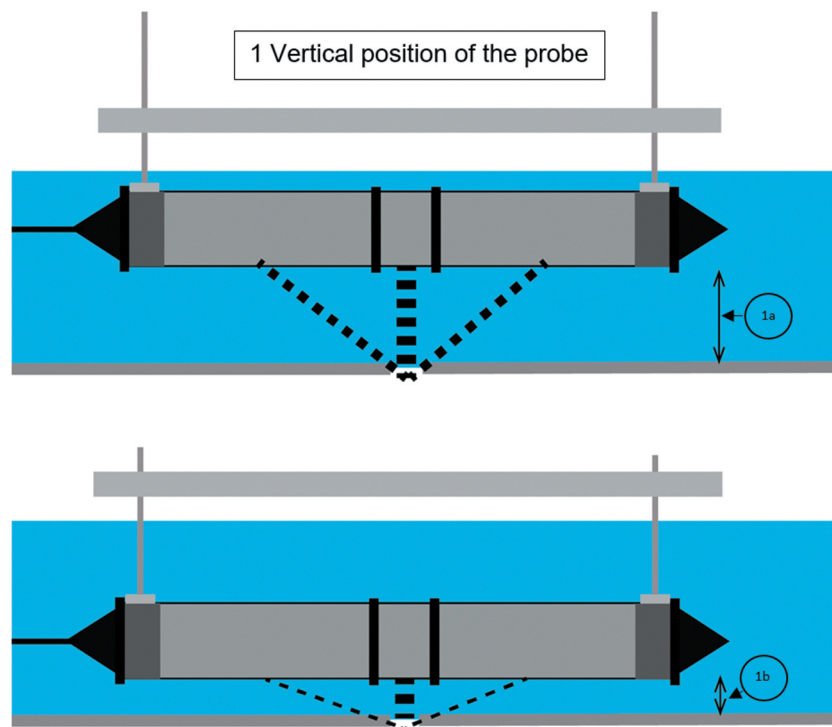
Figure 12. An indication of the electrical current between the electrodes of the probe and the leakage. The dashed lines indicate the main direction and the order of magnitude of the electrical current between the different electrodes of the probe and the leakage. If the vertical position of the probe is reduced (1b); the ratio between the resistances will change since the decrease in distance between the central electrode and the leakage is larger than the decrease in distance between the outer electrodes and the leakage.

and small differences in the physical contact between the grounding pin and the surrounding soil are expected to be responsible for small deviations as well. These deviations can be seen in the linear increase in the resistance with the increasing horizontal distance of the grounding pin to the leakage. When the intrusion depth of the grounding pin is increased, the change in resistance between the leakage and the grounding pin (Yds) and the resistance between the probe and the grounding pin (*Total*) show a deviation. This is rather unexpected since other parameters remain constant. The exact origin of this difference has not been investigated any further, but local conditions around the leak, such as piping and void formation, are likely to contribute to this. These conditions and inhomogeneities cannot be prevented, even under laboratory conditions.

Electrical resistance of the leakage

As expected, a systematic error in the quantification of the electrical resistance of the leakage is observed. Logically, the largest errors can be observed if the resistance between the probe and the grounding pin is assumed to represent the electrical resistance of the leakage. The resistance between the probe and the grounding pin is a factor 3.0–6.5 times higher as the estimated reference electrical resistance of the leakage at the investigated geometries. This error reduces if more information is included in the estimate of the electrical resistance of the leakage. For example, if the resistance of the soil (Yds) is included in the estimate,

the ratio between the obtained resistance of the leakage and the estimated reference electrical resistance of the leakage (Rhr) ranges between 2.0 and 5.5. If the resistances between the electrodes of the probe and the leakage (Ymh, Ylh and Yrh) are also included, the ratio between Rhc and Rhr decreases to 1.1.

The remaining difference between the calibrated electrical resistance of the leakage (Rhc) and the estimated reference resistance of the leakage (Rhr) is likely due to a combination of factors:

- The presence of parasitic capacitances in the experimental set up and the resulting electrical currents are unavoidable. These affect the accuracy of the measurement system. Despite efforts made to reduce the parasitic currents, they are likely to contribute to the observed difference.
- Changes in the conductivity at the leakage location due to flowing water in the leakage itself could affect the electrical resistance of the leakage. This process cannot be measured with the experimental set-up.
- Conditions at the leakage itself are different from the conditions at the adjacent electrode in the soil or water. This is due to the possible inhomogeneity of the sand/water mixture and the possible local temperature differences.

Conclusions

This study aims at validating the required assumptions to quantify leakage with a geo-electrical measurement system.

In total 21 measurement geometries are tested in the experimental set-up. In the experimental set-up the capacitive current at the leakage location is negligible and the maximum current is observed at the leakage location. Depending on the horizontal and vertical position of the probe or the grounding pin, the width and height of the peak in the current-position diagram varies. Additional research is needed to investigate the transferability of the results between different leakage sizes and pipe diameters.

This study demonstrates that the mobile geo-electrical measurement system can detect and accurately locate potential leakages. However, the authors believe that this method in its current application is not suitable to reliably quantify leakage dimensions and/or leakage rates. The results presented in this study do not support the assumption that a change in the current due to a leakage in the pipe is uniquely attributable to the electrical resistance of the leakage. Although not explicitly investigated, the results of this research do not suggest a clear dependency between the measured current and the leak discharge. As indicated by the results; next to the leakage, the water surrounding the probe and the interplay between the central and outer electrodes and the resistance of the soil surrounding the pipe has shown to influence the measured current at the leakage location as well. Consequently, a systematic error is introduced if these components are ignored. The results of the lab set-up demonstrate that the electrical resistance of the leakage is overestimated by a factor of 3.0 to 6.5 at the investigated geometries. Hence, the leakage dimensions are significantly underestimated. Although experiments have been performed at exfiltration conditions only, the authors cannot think of any reason why these findings would not also be valid for infiltrating conditions.

The required additional data to reduce the systematic error is often unknown and/or difficult to obtain in practice. Moreover, to quantify the leakage solely with data from the geo-electrical system, a clear relation between the measured current and the leakage's size and/or discharge must be available. This study shows that the measured current and the resistance is influenced by the distance and depth of the grounding pin and the distance between the probe and the leakage. Leakage dimensions and discharge, however, remain constant. Hence, the required assumptions with respect to the leakage quantification are not easily met, making leakage quantification with the mobile geo-electrical measurement in sewer systems a challenging subject.

Acknowledgements

Data availability statement

The data that support the findings of this study are available from the corresponding author, [B.S], upon reasonable request.

Disclosure statement

No potential conflict of interest was reported by the author(s).

ORCID

Bram Stegeman ⓘD http://orcid.org/0000-0002-1565-2509
Jeroen Langeveld ⓘD http://orcid.org/0000-0002-0170-6721
François Clemens-Meyer ⓘD http://orcid.org/0000-0002-5731-0582

References

ASTM. 2018. "Standard Practice for Locating Leaks in Sewer Pipes by Measuring the Variation of Electric Current Flow through the Pipe Wall 1." *Astm* 13 (Reapproved 2018): 1–7. doi:10.1520/F2550-13R18.

Beheshti, Maryam, and Sveinung Sægrov. 2018. "Quantification Assessment of Extraneous Water Infiltration and Inflow by Analysis of the Thermal Behavior of the Sewer Network." *Water (Switzerland)* 10: 8. doi:10.3390/w10081070.

Davies, J. P., B. A. Clarke, J. T. Whiter, and R. J. Cunningham. 2001. "Factors Influencing the Structural Deterioration and Collapse of Rigid Sewer Pipes." *Urban Water* 3 (1–2): 73–89. doi:10.1016/S1462-0758(01)00017-6.

De Bénédittis, J., and Jean-Luc Bertrand-Krajewski. 2005a. "Infiltration in Sewer Systems: Comparison of Measurement Methods." *Water Science and Technology* 52 (3): 219–227. doi:10.2166/wst.2005.0079.

De Bénédittis, J., and Jean-Luc Bertrand-Krajewski. 2005b. "Measurement of infiltration rates in urban sewer systems by use of oxygen isotopes *Water Science and Technology* 52(3): 229–237. doi:10.2166/wst.2005.0080.

Dirksen, J., F. H L R Clemens, H. Korving, F. Cherqui, P. Le Gauffre, T. Ertl, H. Plihal, K. Müller, and C. T M Snaterse. 2013. "The Consistency of Visual Sewer Inspection Data." *Structure and Infrastructure Engineering* 9 (3): 214–228. doi:10.1080/15732479.2010.541265.

Gokhale, Sanjiv, and Jeffrey A. Graham. 2004. "A New Development in Locating Leaks in Sanitary Sewers." *Tunnelling and Underground Space Technology* 19 (1): 85–96. doi:10.1016/j.tust.2003.08.003.

Henley, Peter, and Chuck Hansen. 2019. "WRc's Use of Focused Electrode Leak Location to Assess Gravity Sewers in the United Kingdom, United States and Germany before and after Trenchless Rehabilitation." In *International No-Dig 2019 37th International Conference and Exhibition*, 690–699. Italy: Florence.

Hoes, O. A.C., R. P.S. Schilperoort, W. M.J. Luxemburg, F. H.L.R. Clemens, and N. C. van de Giesen. 2009. "Locating Illicit Connections in Storm Water Sewers Using Fiber-Optic Distributed Temperature Sensing." *Water Research* 43 (20): 5187–5197. doi:10.1016/j.watres.2009.08.020.

Lee, Do Gyun, Patrick R. Roehrdanz, Marina Feraud, Jared Ervin, Tarun Anumol, Ai Jia, Minkyu Park, et al. 2015. "Wastewater Compounds in Urban Shallow Groundwater Wells Correspond to Exfiltration Probabilities of Nearby Sewers." *Water Research* 85: 467–475. doi:10.1016/j.watres.2015.08.048.

Malik, Abdul Qadir. 2019. "The Use of New Condition Assessment Technologies for Selecting Trenchless Rehabilitation of Wastewater Networks in Ras Al Khaimah, UAE." In *International No-Dig 2019 37th International Conference and Exhibition*, 64–72. Italy: Florence.

Martel, Katherine D, Chris Feeney, and Mary Ellen Tuccillo. 2011. *Field demonstration of condition assessment technologies for wastewater collection systems.* EPA/600/R-11/078 (U.S. Environmental Protection Agency (USEPA)). http://nepis.epa.gov/Exe/ZyPURL.cgi?Dockey=P100C8E0.txt.

Moy, Terry, Charles G. Wilmut, and Robert J. Harris. 2012. "USEPA Sewer Electro Scan Field Demonstration Revisited." In *WEFTEC 2012-85th Annual Technical Exhibition and Conference* New Orleans, Louisiana, USA. doi:10.2175/193864712811741205.

Panasiuk, Oleksandr, Annelie Hedström, Jeroen Langeveld, Cornelis de Haan, Erik Liefting, Remy Schilperoort, and Maria Viklander. 2019. "Using Distributed Temperature Sensing (DTS) for Locating and Characterising Infiltration and Inflow into Foul Sewers Before, during and after Snowmelt Period." *Water (Switzerland)* 11 (8): 1–12. doi:10.3390/w11081529.

Rieckermann, J, V Bareš, O Kracht, D Braun, and W Gujer. 2007. "Estimating Sewer Leakage from Continuous Tracer Experiments." *Water Research* 41 (9): 1960–1972. doi:10.1016/j.watres.2007.01.024.

Selley, Richard C., and Stephen A. Sonnenberg. 2015 Methods of Exploration. *Elements of Petroleum Geology*. Academic Press. doi:10.1016/b978-0-12-386031-6.00003-5.

Selvakumar, Ariamalar, Mary Ellen Tuccillo, Katherine D Martel, John C Matthews, and Chris Feeney. 2014. "Demonstration and Evaluation of State-of-the-Art Wastewater Collection Systems Condition Assessment Technologies." *Journal of Pipeline Systems Engineering and Practice* 5(2):1–11. doi:10.1061/(ASCE)PS.1949-1204.0000161.

Spiegel, Murray. 1974. *Schaum's Outline of Theory and Problems of Fourier Analysis with Applications to Boundary Value Problems*. New York: McGraw-Hill Companies 978-0-07-060219-9.

Stanić, Nikola, Jeroen G. Langeveld, and François H.L.R. Clemens. 2014. "HAZard and OPerability (HAZOP) Analysis for Identification of Information Requirements for Sewer Asset Management." *Structure and Infrastructure Engineering* 10 (11): 1345–1356. doi:10.1080/15732479.2013.807845.

Tscheikner-Gratl, Franz, Nicolas Caradot, Joao P. Frédéric Cherqui, Mehdi Ahmadi Leitão, Jeroen G. Langeveld, Yves Le Gat, Lisa Scholten, et al. 2019. "Sewer Asset Management–State of the Art and Research Needs." *Urban Water Journal* 16 (9): 662–675. doi:10.1080/1573062X.2020.1713382.

Weiß, G., H. Brombach, and B. Haller. 2002. "Infiltration and Inflow in Combined Sewer Systems: Long-Term Analysis." *Water Science and Technology* 45 (7): 11–19. doi:10.2166/wst.2002.0112.

Wolf, Leif. 2003. "Anwendung Einer Segmentierten Geoelektrischen Sonde Zur Leckagendetektion in Abwasserkanälen." *Technisches Messen* 70 (7–8): 346–351. doi:10.1524/teme.70.7.346.22647.

Wood, Warwick, and Derecke Palmer. 2000. "The Application of Mise-a-La-Masse and Resistivity Surveys to the Detection of Pollution from Leaking Sewers." *Exploration Geophysics* 31 (3): 515–519. doi:10.1071/EG00515.

Zhang, Mingkai, Yanchen Liu, David Z. Xun Cheng, Hanchang Shi Zhu, and Zhiguo Yuan. 2018. "Quantifying Rainfall-Derived Inflow and Infiltration in Sanitary Sewer Systems Based on Conductivity Monitoring." *Journal of Hydrology* 558: 174–183. doi:10.1016/j.jhydrol.2018.01.002.

Zhao, Zhichao, Hailong Yin, Xu Zuxin, Jian Peng, and Yu. Ziwen. 2020. "Pin-Pointing Groundwater Infiltration into Urban Sewers Using Chemical Tracer in Conjunction with Physically Based Optimization Model." *Water Research* 175. doi:10.1016/j.watres.2020.115689.

Appendices

Appendix A. Model equations

Model equations and background information are presented in this appendix.

Complex impedance and admittance

Each of the complex impedances (Z) of the electrical circuit is a sum of a real part (Resistance, R) and an imaginary part (Reactance, jX). In general, the complex impedances (Z) are expressed by equation A.1 in which j is the imaginary unit (-).

$$Z = R + jX \tag{A.1}$$

The reactance of a capacitor is expressed by equation A.2, in which C is the capacitance and ω is the radial frequency.

$$X = \frac{1}{\omega \cdot C} \tag{A.2}$$

In the electrical circuit both the resistance and the parallel capacitance of each component are taken into account. Because of the use of admittances (Y, equation A.3), the reciprocal of impedances is more convenient to use. The general form of the admittance with a resistor ($Yres$) in parallel with a capacitor ($Ycap$) can be expressed by equation A.4.

$$Y = \frac{1}{Z} = \frac{1}{R + jX} \tag{A.3}$$

$$Y_{xx} = Y_{res} + Y_{cap} = \frac{1}{R_{xx}} + j \cdot \omega \cdot C_{xx} = \frac{\sqrt{(\omega \cdot R_{xx} \cdot C_{xx})^2 + 1}}{R_{xx}} \tag{A.4}$$

Node equations full model

For each node in the electrical circuit (N_m, N_h, N_s, N_d) a Kirchhoff equation can be written. All currents flow into the nodes. Using Ohm's law, writing the currents as functions of the node voltages (V_m, V_h, V_s, V_d) and the admittances, the equations are given by equation A.5 to A.8.

Node Nd:

$$Y_s \cdot V_s - Y_s \cdot V_d + Y_{ld} \cdot V_m - Y_{ld} \cdot V_d + Y_{ds} \cdot 0^a - Y_{ds} \cdot V_d + Y_{rd} \cdot V_m - Y_{rd} \cdot V_d = 0 \tag{A.5}$$

Node Ns:

$$Y_h \cdot V_h - Y_h \cdot V_s + Y_{ms} \cdot V_m - Y_{ms} \cdot V_s + Y_s \cdot V_d - Y_s \cdot V_s = 0 \tag{A.6}$$

Node Nh:

$$Y_{mh} \cdot V_m - Y_{mh} \cdot V_h + Y_{lh} \cdot V_m - Y_{lh} \cdot V_h + Y_h \cdot V_s - Y_h \cdot V_h + Y_{rh} \cdot V_m - Y_{rh} \cdot V_h = 0 \tag{A.7}$$

Node Nm:

$$Y_{mm} \cdot V_g - Y_{mm} \cdot V_m + Y_{lm} \cdot V_m - Y_{lm} \cdot V_m + Y_{ms} \cdot V_s - Y_{ms} \cdot V_m +$$
$$Y_{mh} \cdot V_h - Y_{mh} \cdot V_m + Y_{rm} \cdot V_m - Y_{rm} \cdot V_m + Y_{ia} \cdot 0^a - V_m \cdot Y_{ia} = 0 \tag{A.8}$$

Solving this system of equations (A.5 to A.8) for V_m, V_s, V_h, V_d results in respectively equation A.9, A.10, A.11 and A.12.

$$V_m = \frac{V_g \cdot Y_{mm}}{Y_{ia} + Y_{mh} + Y_{mm} + Y_{ms} - \frac{Y_{ms} \cdot T_1}{T_2} - \frac{Y_{mh} \cdot \left(Y_{lh} + Y_{mh} + Y_{rh} + \frac{Y_h \cdot T_1}{T_2}\right)}{Y_h + Y_{lh} + Y_{mh} + Y_{rh}}} \tag{A.9}$$

Where:

$$T_1 = Y_{ms} + \frac{Y_h \cdot (Y_{lh} + Y_{mh} + Y_{rh})}{Y_h + Y_{lh} + Y_{mh} + Y_{rh}} + \frac{Y_s \cdot (Y_{ld} + Y_{rd})}{Y_{ds} + Y_{ld} + Y_{rd} + Y_s}$$

$$T_2 = Y_h + Y_{ms} + Y_s - \frac{Y_h^2}{Y_h + Y_{lh} + Y_{mh} + Y_{rh}} - \frac{Y_s^2}{Y_{ds} + Y_{ld} + Y_{rd} + Y_s}$$

$$V_s = \frac{V_m \cdot Y_{ms} + \frac{V_m \cdot Y_s (Y_{ld} + Y_{rd})}{Y_{ds} + Y_{ld} + Y_{rd} + Y_s} + \frac{V_m \cdot Y_h (Y_{lh} + Y_{mh} + Y_{rh})}{Y_h + Y_{lh} + Y_{mh} + Y_{rh}}}{Y_h + Y_{ms} + Y_s - \frac{Y_h^2}{Y_h + Y_{lh} + Y_{mh} + Y_{rh}} - \frac{Y_s^2}{Y_{ds} + Y_{ld} + Y_{rd} + Y_s}} \tag{A.10}$$

$$V_h = \frac{V_m(Y_{lh} + Y_{mh} + Y_{rh}) + \frac{Y_h \left(V_m \cdot Y_{ms} + \frac{V_m \cdot Y_s (Y_{ld} + Y_{rd})}{Y_{ds} + Y_{ld} + Y_{rd} + Y_s} + \frac{V_m \cdot Y_h (Y_{lh} + Y_{mh} + Y_{rh})}{Y_h + Y_{lh} + Y_{mh} + Y_{rh}}\right)}{Y_h + Y_{ms} + Y_s - \frac{Y_h^2}{Y_h + Y_{lh} + Y_{mh} + Y_{rh}} - \frac{Y_s^2}{Y_{ds} + Y_{ld} + Y_{rd} + Y_s}}}{Y_h + Y_{lh} + Y_{mh} + Y_{rh}} \tag{A.11}$$

$$V_d = \frac{V_m(Y_{ld} + Y_{rd}) + V_s \cdot Y_s}{Y_{ds} + Y_{ld} + Y_{rd} + Y_s} \tag{A.12}$$

Subsequently, the measured current can be written as:

$$I_m = (V_g - V_m) \cdot Y_{mm} \tag{A.13}$$

aGround

Appendix B. Measurement geometries

The laboratory experiments have been done at 21 measurement geometries. Detailed information of each geometry is presented in Table B1.

Table B1. Measurement geometries.

Geometry (Nr.)	Vertical distance bottom probe-leakage (m)	Depth grounding pin (m)	Horizontal distance grounding pin – leakage (m)
1	0.035	0.30	0.500
2	0.025	0.30	0.500
3	0.015	0.30	0.500
4	0.045	0.30	0.500
5	0.055	0.30	0.500
6	0.065	0.30	0.500
7	0.075	0.30	0.500
8	0.035	0.30	0.500
9	0.035	0.30	0.650
10	0.035	0.30	0.350
11	0.035	0.30	0.800
12	0.035	0.30	0.200
13	0.035	0.30	0.425
14	0.035	0.30	0.575
15	0.035	0.50	0.500
16	0.035	0.50	0.650
17	0.035	0.50	0.350
18	0.035	0.50	0.800
19	0.035	0.50	0.200
20	0.035	0.50	0.425
21	0.035	0.50	0.575